

Experimental Verification of Constitutive Equations for Creep and the Interaction of Creep and Plasticity Under Biaxial Loading Conditions

F. Roode

*TNO, Institute for Mechanical Constructions,
P.O. Box 29, NL-2600 AA Delft, The Netherlands*

W. Dortland

TNO, Metal Research Institute, P.O. Box 541, NL-7300 AM Apeldoorn, The Netherlands

SUMMARY

More than 80 creep experiments have been carried out on the austenitic steel WN 1.4948 (18 Cr-11 Ni steel similar to AISI 304 SS). These experiments were intended to arrive at sufficiently accurate and experimentally verified constitutive equations for creep deformations arising from arbitrary loading conditions. The test programme did consist of constant load and programme loading creep tests on solid specimens, including relaxation and recovery parts as well as stepwise increasing and decreasing loads. Furthermore tubular specimens were submitted to loading programmes that were combinations of an axial load, torsional load and internal pressure, thus covering the complete range of principal stress ratios $-1 \leq \sigma_1/\sigma_2 \leq 1$. The constitutive equations were based on the so-called fraction model, originally formulated by BESSELING.

In this model a volume element is thought to be subdivided into a set of parallel volume fractions. Each of these volume fractions exhibits a purely isotropic material behaviour and can describe elastic behaviour and primary and secondary (non-recoverable) creep deformations.

The combination of the parallel volume fractions will introduce a kinematic hardening (recoverable) creep deformation.

For a number of typical creep experiments, the experimental results will be compared with theoretical predictions according to the fraction model.

Some discussion will be dedicated to the commonly observed scatter in creep data and on the parameters that have been found to influence this scatter.

1. Introduction

One of the major problems in obtaining realistic analysis results in high temperature technology is the need to have a sufficiently accurate characterization of the material behaviour given by the constitutive equations. Furthermore these constitutive equations should be formulated in such a way that they can be implemented easily in arbitrary finite element computer codes.

In order to meet these demands a TNO-research programme on inelastic analysis of structural components is in progress. In this research programme a number of aspects related to inelastic analysis are investigated.

- Development, verification and qualification of finite element computer codes. In this research programme not only computer codes are developed, but these computer codes are also verified by performing benchmark calculations with these computer programmes and with various constitutive equations (including classical models and the fraction model). A part of this research is reported by KONTER and KUSTERS [1].
- Constitutive equations for plastic deformation. The constitutive equations for plasticity have been based on the so-called fraction model originally formulated by BESSELING [2]. For the verification of these constitutive equations, more than forty biaxial plasticity experiments have been carried out. These tests were performed at room temperature and the tests have been carried out in such a way that time dependent effects were reduced as much as possible. A part of this research is reported by JANSSEN and HUETINK [3].
- Constitutive equations for creep deformations and for the combination of creep and plastic deformation. In this research programme creep experiments have been carried out at a constant temperature in the temperature range of 525-600°C. The major parts of these experiments have been carried out in such a way that time independent effects (plasticity) were reduced as much as possible. In the last part of the research programme a number of tests have been performed where cyclic plastic deformation was followed by creep deformation and visa-versa. These tests were intended to study the interaction between plastic deformation and creep deformation.

The research programme on constitutive equations was carried out on an austenitic 18 Cr-11 Ni steel and on a niobium stabilized 2½ Cr-1 Mo steel (in German standard indicated as respectively WN 1.4948 and WN 1.6770). In this paper only the research on WN 1.4948 will be presented and furthermore only the inelastic behaviour at a constant temperature of 550°C will be dealt with.

2. Experiments

For the uniaxial creep experiments solid test specimens as shown in Figure 1a were used. An exception to this rule was formed by the tension/compression tests, where tubular specimens were used. The biaxial experiments were performed on tubular specimens. Figure 1b shows such a tubular specimen which has been used for combinations of axial load and internal pressure. For loading programmes which included torsional loads a test specimen similar to the one in Figure 1b was used but with half the gauge length (50 mm). Two different types of testing machines were used for uniaxial and biaxial creep experiments respectively.

Uniaxial creep tests

The uniaxial creep testing machines for uniaxial tension tests on solid specimens and

for uniaxial push/pull tests on tubular specimens are semi-deadweight types with a single lever, a travelling weight of 1000 N, a lever ratio of 30:1, and thus a maximum load of 30 kN. The machine is provided with a resistance furnace with three separate adjustable zones. To measure the temperatures three Pt-10% Rh thermocouples were fastened on the gauge length of the specimen. Strain measurements were carried out by a mechanical extensometer existing of a couple of rods clamped on the specimen and supplied with two linear variable displacement transducers outside the furnace. A special device has been designed, located on the inner side of the tubular specimen, to be able to change the direction of loading (compression).

Biaxial creep tests

A completely new test rig had to be designed for the creep tests under combinations of axial load, torsional load and internal pressure. Figures 2 and 3 give an impression of this test facility. The biaxial creep testing machine is a semi deadweight type with single levers and the following specification.

- axial load : lever ratio \pm 1:20 (maximum load 10 kN)
- torsional load : lever ratio \pm 1:20 (maximum couple 600 Nm)
- internal pressure system (with air) : maximum 250 bar
- sensitivity for the torsion angle : 0,001° (range of measurement \pm 10°)
- sensitivity for a change in length : 0,001 mm (0,002%); range \pm 10 mm

The deadweights at the end of the levers are barrels filled with water (automatically emptied at relaxation tests).

The heating and temperature control is similar to the uniaxial machines. Axial strain and shear deformation measurements were carried out by a mechanical extensometer provided with rods, ball bearings, frame and so on (see Fig. 4), clamped on the specimens and supplied with nine linear variable displacement transducers outside the furnace. At one horizontal cross-section of the specimen the change of diameter was measured with 6 inductive transducers at intervals of 60° (3 diameters).

In all the experiments extreme precautions were taken to ensure that the influence of parameters, which were known to have an effect on the scatter in creep data [7], was reduced as much as possible.

- The temperature variation of all experiments was within \pm 1°C for the total test period.
- The test machines were located in a conditioned room with ample provisions to ensure that no vibrations in the building could be transferred to the test facility.
- The test specimens were planned to be loaded in such a way that a constant nominal stress rate of 12,5 N/mm²/min was achieved; furthermore loads and strains were measured continuously during this period.
- Finite element calculations were performed for all test specimens (including plastic and creep deformation) to ensure that no strain concentrations would occur within the gauge length of the specimen.
- To avoid bending stresses severe restrictions were put on the tolerances for out of roundness and wall thickness. Furthermore the axial load was transmitted by means of cardanic fastenings via mounting ridges to the tubular specimens. Apart from that the displacement measurements were conducted in such a way that bending effects could be traced.
- The temperature control system was tested and calibrated extensively.

3. Constitutive equations

As already mentioned previously, the constitutive equations for creep are based on the so-called fraction model. A uniaxial representation of this model is given in Figure 5. In this model a volume element is thought to be subdivided into a number of volume fractions, and furthermore the total strain is assumed to be the same for all volume fractions. Although there is no limitation to the number of volume fractions, only two fractions are used in the present model. The creep behaviour in a volume fraction, which is represented by the dashpots in Figure 5, is assumed to be completely isotropic. The definition of the creep model for each volume fraction k is based on rather classical assumptions. A basic postulate is the existence of an energy dissipation function f^k for each volume fraction, which can also be written as a function of an equivalent stress $\bar{\sigma}^k$ and an equivalent creep strain rate $\dot{\epsilon}_c^k$.

$$f^k = \sigma_{ij}^k \cdot (\dot{\epsilon}_{ij}^k)_c = \bar{\sigma}^k \cdot \dot{\epsilon}_c^k \quad (1)$$

Furthermore it is assumed that the energy dissipation function can only be a function of the equivalent stress $\bar{\sigma}^k$, the temperature T and some hardening parameter η^k . The assumption that the creep strain rate $(\dot{\epsilon}_{ij}^k)_c$ is normal to the surface of constant rate of dissipation [6] leads to the following equation (under constant temperature condition).

$$(\dot{\epsilon}_{ij}^k)_c = \mu^k \frac{\partial f^k}{\partial \sigma_{ij}^k} = \mu^k \left[\frac{\partial f^k}{\partial \bar{\sigma}^k} + \frac{\partial f^k}{\partial \eta^k} \frac{\partial \eta^k}{\partial \bar{\sigma}^k} \right] \frac{\partial \bar{\sigma}^k}{\partial \sigma_{ij}^k} \quad (2)$$

With the use of Eq. (1) μ^k can be eliminated leading to an equation for the creep strain rate which still depends on the definition of f^k ($\bar{\sigma}^k, T, \eta^k$) and $\bar{\sigma}^k$.

In defining the equivalent stress $\bar{\sigma}^k$, the observation that the change of volume during creep is negligible has been used, leading to the commonly accepted hypothesis that the hydrostatic stress has no influence on the creep behaviour [5]. The equivalent stress $\bar{\sigma}^k$ was therefore formulated as an equivalent VON MISES stress. The non-hardening part of the creep strain rate was assumed to be governed by a stress dependent power law, whereas the hardening part of the creep strain rate was taken to be a saturating hardening type, leading to a rather classical formulation:

$$\dot{\epsilon}_c^k = \left\{ \bar{\epsilon}_{t_0}^k \cdot R \cdot e^{-R \cdot h^k} - \left(\frac{\bar{\sigma}^k}{\bar{\sigma}_k} \right)^n \right\} \cdot \frac{dh^k}{dt} \quad (3)$$

In this equation h^k is a strain hardening parameter with the dimension of time ($h^k = 0$ at $t = 0$).

The first part of this equation can be seen as a primary creep strain rate where R is the same for all volume fractions and

$$\bar{\epsilon}_{t_0}^k = \bar{\epsilon}_{t_1}^k \cdot (\bar{\sigma}^k - \bar{\sigma}_0) \quad (4)$$

where both $\bar{\epsilon}_{t_1}^k$ and $\bar{\sigma}_0$ are the same for all volume fractions.

Further the parameter n in the second part of Eq. (3) (secondary creep strain rate) is

also assumed to be equal for all volume fractions. In comparison with previous formulations of the fraction model for creep [2,4] the model has been changed by introducing a primary creep strain rate on the fraction level and by taking the parameter n to be equal for all volume fractions. The formulation of this model in combination with plasticity is presented in [1] and [3].

4. Evaluation and verification of the model

The two-fraction model for creep contains 7 parameters, namely n , R , $\bar{\epsilon}_{t1}$ and $\bar{\sigma}_0$ which are the same for both volume fractions and the volume fraction size ψ_1 and the stresses σ^{*1} and σ^{*2} . The parameters n , R and $\bar{\sigma}_0$ have been determined by plotting the secondary creep strain rate and the primary creep as a function of the applied stress (see Figs. 6 and 7). As can be seen in Figure 7, the scatter in primary creep strains is rather large. Therefore only a linear stress dependency was assumed for the primary creep strain Eq. (4). Furthermore R was taken to be a constant.

The parameters ψ_1 , σ^{*1} and σ^{*2} have been estimated from one constant load experiment under the assumption that the fraction model was purely kinematic ($\bar{\epsilon}_{t1} = 0$). For the determination of these parameters the creep strain rate at the beginning of the experiment, the secondary creep strain rate and the total creep strain at a certain point in time had to be known. Finally the parameter ϵ_{t1} , σ^{*1} and σ^{*2} were determined from a cyclic creep test (with equal creep periods in the positive and negative direction) thus establishing a correct ratio between isotropic and kinematic hardening. The numerical values of the parameters are given in Figure 5.

With this model a number of experiments have been analysed. First of all it had to be concluded that there was a scatter in creep data (see Fig. 8). Practically all of this scatter was due to differences in primary creep strain. The cause for this scatter could be found in the fact that the stress rate at loading of the test specimen was not very constant. This can be seen in Figure 9 where the initial stress strain curves for various experiments are plotted. Therefore a number of experiments were selected for which the stress strain curves indicated that the stress rate was reasonably constant. A comparison between theoretical and experimental results for these experiments and various loading conditions is given in Figure 10-13. As can be seen in these figures the differences between theory and experiments are quite acceptable.

Differences in primary creep strains have only an effect on the parameter ϵ_{t1} in the fraction model. This means that even if different values of ϵ_{t1} are used the model will show the same deformation behaviour as soon a secondary creep stage is reached (isotropic hardening is saturated). This is in complete agreement with experimental observations which show that the scatter is far less after the first part of the experiment (Fig. 14). Furthermore this phenomenon indicates that plastic deformations hardly have any influence on the subsequent creep deformation.

5. Conclusions

- The present fraction model shows an acceptable agreement with experimental results for various loading programme as long as the initial loading condition are kept under control.

- The use of a VON MISES equivalent stress proves to be sufficiently accurate to describe multiaxial creep deformation for this material.
- The scatter in creep data are mostly caused by differences in initial loading conditions, furthermore this scatter is only present in the primary creep strain at the beginning of the experiment.
- The scatter in creep data only has one influence on one parameter (ϵ_{t1}) in the fraction model. Our present investigations seem to indicate that it is very well possible to relate this parameter to the loading histories prior to the creep period.

Acknowledgement

This work was commissioned by the Project Group of Nuclear Energy TNO. The authors wish to thank the Project Group and the Dutch Ministry of Economic Affairs for the permission to publish this paper.

References

- [1] KONTER, A.W.A., KUSTERS, G.M.A., "Influence of constitutive equations on the results of inelastic analyses of benchmark problems", Proc. 6th Int. Conf. on Structural Mechanics in Reactor Technology, paper M 3/3, Paris, France, (August 17-21, 1981).
- [2] BESSELING, J.F., "A theory of elastic, plastic and creep deformation of an initially isotropic material showing strain hardening, creep recovery and secondary creep". J. Appl. Mech., Vol. 25, No. 4, Dec. 1958, pp. 529-536.
- [3] JANSSEN, G.T.M., HUETINK, J., "Experimental verification of constitutive equations for plasticity under biaxial, cyclic and non-radial loading conditions". Proc. 6th Int. Conf. on Structural Mechanics in Reactor Technology, paper L 4/2, Paris, France, (August 17-21, 1981).
- [4] MEIJERS, P., JANSSEN, G.T.M. and BOOIJ, J., "Numerical plasticity and creep analysis based on the fraction model and experimental verification for AISI 304". Smirt III, paper L 3/9, LONDON (1975).
- [5] BAILEY, R.W., "The utilization of creep test data in engineering design", Proc. Inst. Mech. Engrs., 131, pp. 131-149, (1935).
- [6] ZIEGLER, H., "Zwei Extremalprinzipien der irreversiblen Thermodynamik", Ingenieurs Archive, 30, 410-416, (1961).
- [7] PENNY, R.K., MARRIOT, D.L., "Design for Creep", McGraw-Hill Book Company (UK) Limited, pp. 251-255, (1971).

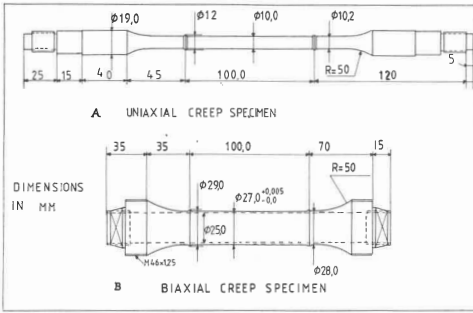


Figure 1 Solid- and tubular test specimen used in the uniaxial- and biaxial creep experiments

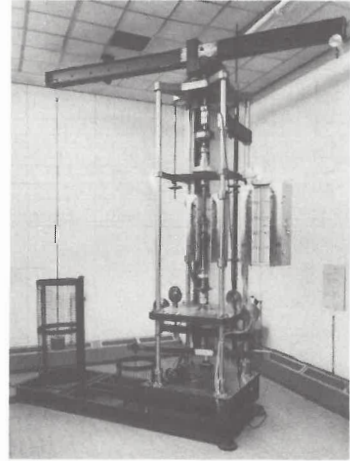


Figure 2 The biaxial creep testing machine

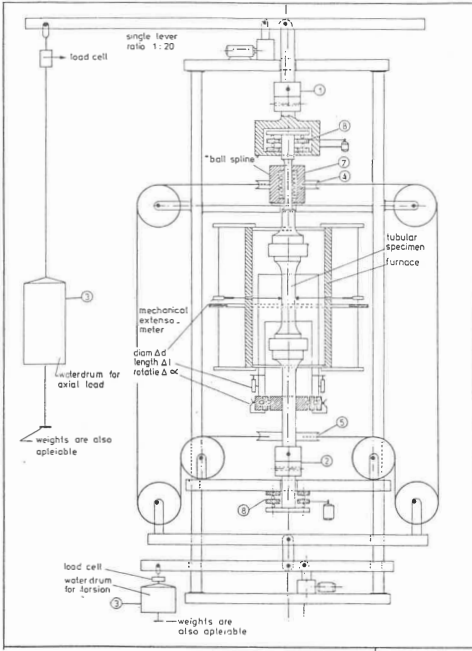


Figure 3 Schematic representation of the biaxial creep testing machine

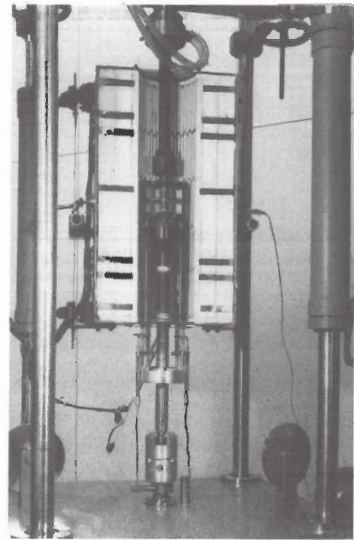


Figure 4 Extensometer configuration for the measurement of elongation and shear angle

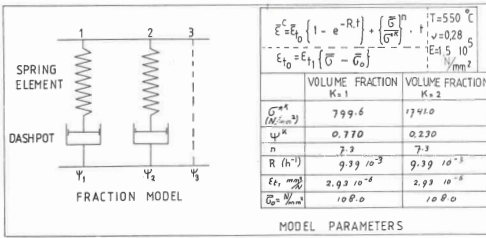


Figure 5

Uniaxial representation of the fraction model and the parameters used in the calculations

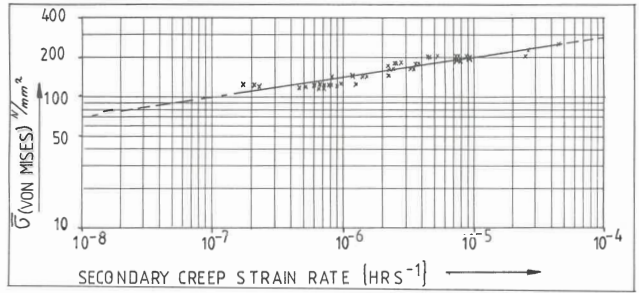


Figure 6 Secondary creep strain rate as a function of the equivalent stress

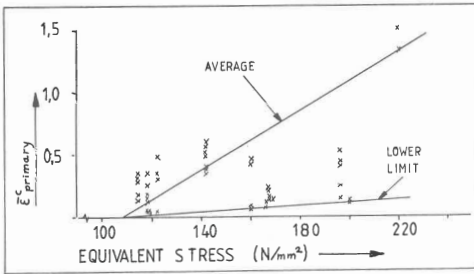


Figure 7 Equivalent primary creep strain as a function of the equivalent stress

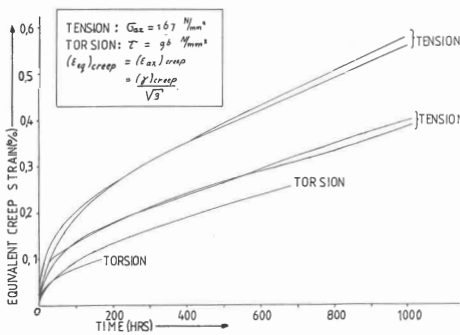


Figure 8 Creep curves for various tests with the same equivalent stress levels

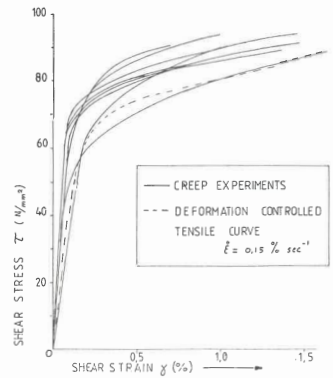


Figure 9 Stress strain curves (initial loading) for various torsion tests

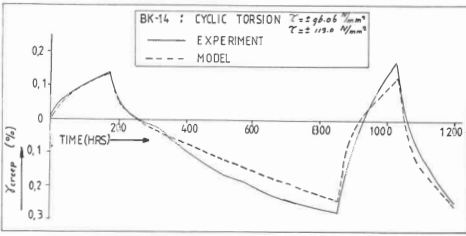


Figure 10 Comparison of experiment and theoretical predictions for a cyclic torsion test

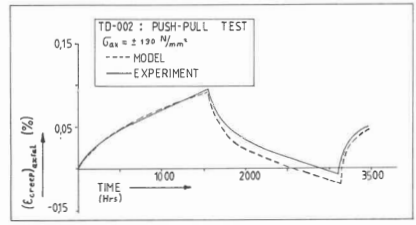


Figure 11 Comparison of experiment and theoretical prediction for a push-pull test

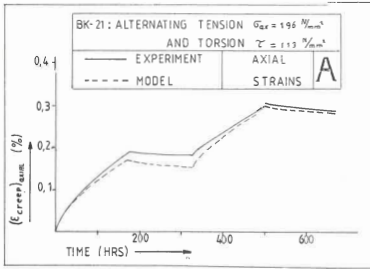


Figure 12a Comparison of theoretical and experimental axial creep strains for an alternating tension-torsion test

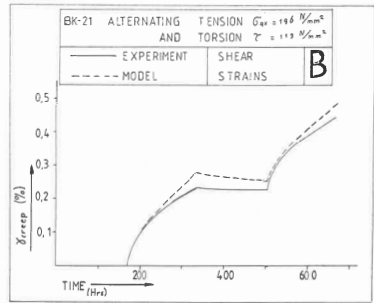


Figure 12b Comparison of theoretical and experimental torsion creep strain for an alternating tension-torsion test

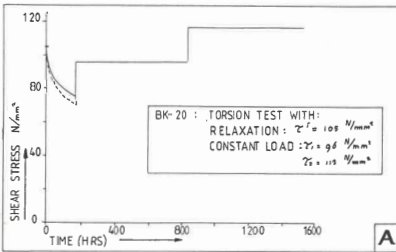


Figure 13a Comparison of the theoretical and experimental loading histogram for a uniaxial creep test

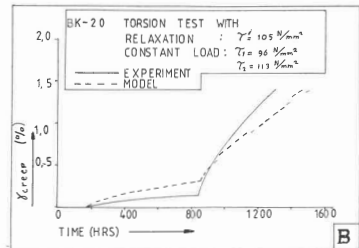


Figure 13b Comparison of theoretical predictions and experiments for a uniaxial creep test

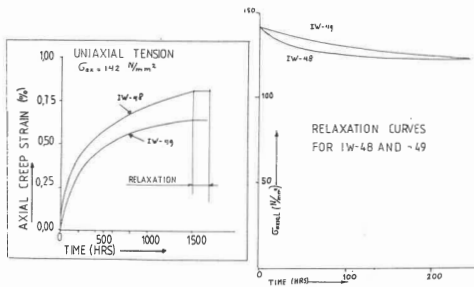


Figure 14 Comparison of two creep tests showing some scatter in the first part of the experiment

